Effect of nanometric grain size on electronic-transport, magneto-transport and magnetic properties of $La_{0.7}Ba_{0.3}MnO_3$ nanoparticles

2008 J. Phys.: Condens. Matter 20 385203

(http://iopscience.iop.org/0953-8984/20/38/385203)

J. Phys.: Condens. Matter **20** (2008) 385203 (12pp) doi:10.1088/0953-8984/20/38/385203

Effect of nanometric grain size on electronic-transport, magneto-transport and magnetic properties of $La_{0.7}Ba_{0.3}MnO_3$ nanoparticles

S K Mandal[1], T K Nath[1,3] and V V Rao[2]

[1] Department of Physics and Meteorology, Indian Institute of Technology Kharagpur, 721302, W.B., India
[2] Cryogenic Engineering, Indian Institute of Technology Kharagpur, 721302, W.B., India

E-mail: tnath@phy.iitkgp.ernet.in

Received 12 January 2008, in final form 27 July 2008
Published 21 August 2008
Online at stacks.iop.org/JPhysCM/20/385203

Abstract

We have investigated the effect of nanometric grain size on electronic-transport, magneto-transport and magnetic properties of single-phase $La_{0.7}Ba_{0.3}MnO_3$ (LBMO) nanoparticles having an average grain size in the nanometric regime (21–35 nm). We have observed that both the metal–insulator transition temperature (T_P) and para-ferromagnetic transition temperature (T_C) shift to lower temperature with a decrease in average grain size. For the entire series of samples, a distinct minima in resistivity at a temperature (T_{min}) followed by an upturn at a very low temperature ($\leqslant$47 K) is observed. We have attributed the steeper low temperature ($\sim$47 K) resistivity upturn in the smaller grain size sample than that in the larger grain size sample below T_{min} to the increased value of charging energy (E_C). E_C has been estimated to be 1.3, 0.56 and 0.04 K for an average grain size of 21, 25 and 30 nm, respectively. Magneto-transport measurements show that the magnitude of low field MR (LFMR) varies with average grain size. In order to investigate the MR behavior of LBMO nanoparticles, we have analyzed our data in the light of a phenomenological model, based on spin-polarized transport of conduction electrons at the grain boundaries. Magneto-transport measurements show that the magnitude of low field MR (LFMR), as well as of high field MR (HFMR), remains constant up to sufficiently high temperature ($\sim$50 K) and then drops sharply with temperature. We found that this strange temperature dependence of MR is decided predominantly by the nature of the temperature response of the surface magnetization (M_S) of nanosized magnetic particles.

(Some figures in this article are in colour only in the electronic version)

1. Introduction

The mixed valence oxide of $R_{1-x}A_xMnO_3$ type, where R is a trivalent rare earth element such as La, Pr or Nd and A is a divalent alkaline earth element such as Ba, Sr or Ca, has been a subject of scientific investigation for many decades [1, 2]. The interest in the perovskite Mn oxides is associated with the colossal magnetoresistance (CMR) effect, which is observed in certain compounds in this class of materials near room temperature. Besides being merely interested in a fundamental understanding of this CMR effect, studies have also been motivated in this class of materials for the possible application of them as magnetic field sensors and other device applications [3–7]. A large number of studies of the CMR effect in this class of materials have been carried out in the case of single crystals [8, 9], thin films [10–12] and ceramic CMR materials [13–15] in both a search for the correct model to explain their magnetic, electrical and magneto-transport properties and the possible application of them as magnetic sensors. These physical properties of

[3] Author to whom any correspondence should be addressed.

perovskite manganites are found to be strongly dependent on doping (x) [16], oxygen stoichiometry [17], average A site ionic size (influencing bond distance d between Mn and O, and bond angle between Mn and O), variance [18] of substituted ions, electronic phase separation [19], etc. Although transition metal oxides with the perovskite structure have a long history of research and have been known as materials with a variety of interesting physical properties, such as electronic-transport, magnetic, dielectric and optical properties, focused research effort on these materials were not made until the report of a room temperature large magnetoresistive effect of 230% at 6 T in half-metallic highly spin-polarized $La_{2/3}Ba_{1/3}MnO_3$ compounds [20] in 1993.

Basically, $La_{0.7}Ba_{0.3}MnO_3$ (LBMO) is one of the prototypical colossal magnetoresistive materials with largest ionic size mismatch between La (1.26 Å) and Ba (1.47 Å) [21]. The phase diagram of this compound $La_{1-x}Ba_xMnO_3$ ($0 \leqslant x \leqslant 1$) was established for the first time through magnetization ($5\ \text{K} \leqslant T \leqslant 360\ \text{K}$, $-7\ \text{T} \leqslant H \leqslant 7\ \text{T}$) and electrical resistivity ($100\ \text{K} \leqslant T \leqslant 400\ \text{K}$) measurements by Ju *et al* [25]. According to this phase diagram, LBMO is supposed to undergo a phase transition from paramagnetic insulator to ferromagnetic metal at approximately $T \sim 330$ K. Recently, Trukhanon *et al* [23] has established a magnetic phase diagram for anion-deficient $La_{1-x}Ba_xMnO_{3-x/2}$ ($0 \leqslant x \leqslant 0.50$) manganites. A giant volume magnetostriction and colossal magnetoresistance is observed for LBMO single crystals in a magnetic field of 8.2 kOe, as reported by Demin *et al* [22]. In a separate study, $La_{0.5}Ba_{0.5}MnO_3$ single-crystalline nanowires were synthesized by a hydrothermal method at low reaction temperature with cubic perovskite structure, where enhanced magnetoresistance (MR) is observed [24]. In recent work [26], it was shown how modified surface magnetization of LSMO nanoparticles can tune the temperature-dependent property of low field MR (LFMR), appearing from a spin-polarized tunneling mechanism.

Although a number of such investigations of the grain size (in the nanometric regime) effect on electrical, magnetic and magneto-transport properties of $La_{1-x}A_xMnO_3$ (A = Sr and Ca) have been recently published [5, 27–38], there has been no systematic investigation of the grain size effect on magneto-transport and electronic-transport properties of LBMO nanoparticles so far. Against this background, we have carried out a systematic investigation of the structural, electronic-transport, magneto-transport and magnetic properties of a series of LBMO nanoparticles having varying grain sizes. An electronic-transport study on this series of LBMO nanoparticles reveals that the metal–insulator transition temperature (T_P) shifts toward lower temperature with decreasing grain size, associated with a pronounced increase in resistivity. Moreover, there is a resistivity upturn in the very low temperature regime (~47 K), which is much steeper for a smaller grain size sample than that of a larger grain size sample. Additionally, we have performed a detailed study of the effect of nanometric grain size on magneto-transport properties of this series of LBMO nanoparticles. We have observed different grain size dependences of LFMR in different magnetic field regimes and have analyzed our data using a phenomenological model [4] based on the spin-polarized tunneling (SPT) of conduction electrons at the grain boundaries. Magneto-transport measurements show that the magnitude of low field MR (LFMR), as well as of high field MR (HFMR), remains constant up to sufficiently high temperature (~50 K) and then drops sharply with temperature. Magnetic study shows that the paramagnetic to ferromagnetic transition temperatures (T_C) of those series of samples shift towards lower temperature with the decrease in average grain size.

2. Experimental details

Nanometric particles of LBMO were prepared from high-purity La_2O_3, $Ba(NO_3)_2 \cdot 6H_2O$ and $C_4H_6MnO_4$ by a chemical 'pyrophoric reaction process'. We have employed an aqueous solution of the requisite amounts of the compounds in distilled water in stoichiometric proportions. Then triethanolamine (TEA) is added to these solutions in such a way that the metal ions to TEA ratio in the starting solutions are maintained at 1:1:4 (La, Ba:Mn:TEA = 1:1:4) to make a viscous solution. The clear solutions of TEA complex metal nitrates are evaporated on a hot plate at 190 °C with constant stirring. The continuous heating of these solutions causes foaming and puffing. During evaporation, the nitrate ions provide an *in situ* oxidizing environment for TEA, which partially converts the hydroxyl groups of TEA to carboxylic acids. When complete dehydration occurs, the nitrates themselves are decomposed with the evolution of brown fumes of NO_2, leaving behind a voluminous, carbonaceous, organic-based, black, fluffy powder, i.e. precursor powder with the desired metal ions embedded in its matrix. The chemical reactions involved in this method are as follows:

$$\begin{aligned}
&0.7\ La_2O_3 + 0.3Ba(NO_3)_2 + C_4H_6MnO_4 + N(CH_2CH_2OH)_3 \\
&\quad \rightarrow\ [La\text{–}N(CH_2CH_2OH)_3]^{2+} + [Ba\text{–}N(CH_2CH_2OH)_3]^{2+} \\
&\qquad + [Mn\text{–}N(CH_2CH_2OH)_3]^{2+} + NO_3^- \\
&\quad \rightarrow\ \text{Oxidation in air} \rightarrow\ La_{0.7}Ba_{0..3}MnO_3\ \text{(nanosized)} \\
&\qquad + CO_2 + NO_2 + N_2 + H_2O.
\end{aligned}$$

The dried carbonaceous mass is then ground to fine powder and calcined at various temperatures (850–1050 °C) to get a series of LBMO nanocrystalline powders.

Structural characterization of the nanocrystalline LBMO powders is carried out using x-ray powder diffraction (XRD) (Models PW 1710 and PW 1810, Philips) with monochromatic Cu Kα radiation ($\lambda \sim 1.542$ Å) and by transmission electron microscopy (TEM) (JEOL, JEM-2100, 200 kV). High resolution field-emission scanning electron microscopy (FE-SEM) and energy-dispersive x-ray (EDAX) analysis have been done using a Carl Zeiss SMT Ltd SUPRA™ 40. The dc voltage is measured for resistivity and MR measurements using the four-probe method by a Keithley 181 nanovoltmeter attached to an Advantest TR6142 programmable dc voltage/current generator. A calibrated Si diode (DT-470) temperature sensor attached to a temperature controller is used for temperature measurement of the samples. Measurements are carried out in a temperature range of 4–300 K using a

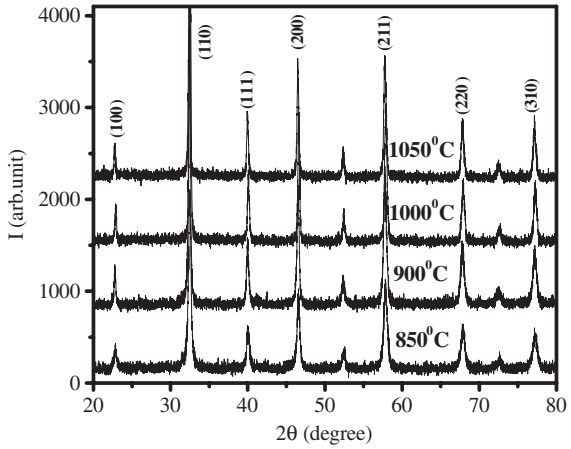

Figure 1. XRD patterns of a series of $La_{0.7}Ba_{0.3}MnO_3$ nanoparticles calcined at 850, 900, 1000 and 1050 °C having average grain sizes 21, 25, 30 and 35 nm, respectively.

helium closed-cycle variable temperature cryostat. MR is measured in the magnetic field range of 0–+5 T using a superconducting magnet along with a magnet power supply (Cryomagnetics). The accuracy of the MR measurement is 1 part in 10 000 Ω in the measured temperature range. Room temperature magnetization versus field measurements of those samples have been done using a home-made vibrating sample magnetometer (VSM). Temperature-dependent permeability measurements of those nanometric samples have been carried out using an LCR meter and a PID controlled variable-temperature cryostat.

3. Results and discussion

3.1. Structural characterization of the samples

Structural characterizations have been carried out through XRD patterns, TEM and high resolution FE-SEM micrographs. XRD patterns of LBMO nanoparticles calcined at 850, 900, 1000 and 1050 °C are shown in figure 1. Peaks were indexed on the basis of a pseudocubic cell. We have estimated the average grain size (D) of those samples through the Debye–Scherrer formula employing the equation $D = 0.89\lambda/(\beta_{\text{eff}} \cos\theta)$, where $\beta_{\text{eff}}^2 = \beta_{\text{sa}}^2 - \beta_{\text{si}}^2$, using the Gaussian peak fit on XRD patterns and $\lambda(= 1.542$ Å), the wavelength of the x-rays used. Here β_{sa} is the full width at half maximum (FWHM) of a particular XRD peak of our samples, β_{si} is the FWHM of a peak of a very high quality Si single crystal and β_{eff} is the effective FWHM of the same XRD peak of our sample. The average grain sizes of those samples are found to be 21, 25, 30 and 35 nm, corresponding to calcination temperatures of 850, 900, 1000 and 1050 °C, respectively.

High resolution FE-SEM of LBMO nanoparticles calcined at 850, 1000 and 1050 °C are shown in figure 2. These micrographs show that particles are in the nanometric regime. The micrograph at a calcination temperature of 1050 °C shows the clear coexistence of two types of grains. One is comparatively smaller in size, whereas other is comparatively larger in size. Although the sample calcined at 1000 °C also exhibits the tendency of having two types of grains, the sample calcined at 850 °C shows almost the same type of grains throughout. The low magnification bright-field TEM micrograph for LBMO nanoparticles calcined at 900 °C is shown in figure 3(a), indicating the nanometric particle size distribution. The selected-area electron diffraction (SAED) patterns for the same sample show a ring-shaped nature (as shown in figure 3(b)), thus indicating a polycrystalline sample. The nominal elements are determined by EDAX analysis as shown in figure 4 for the average grain size of 21 nm.

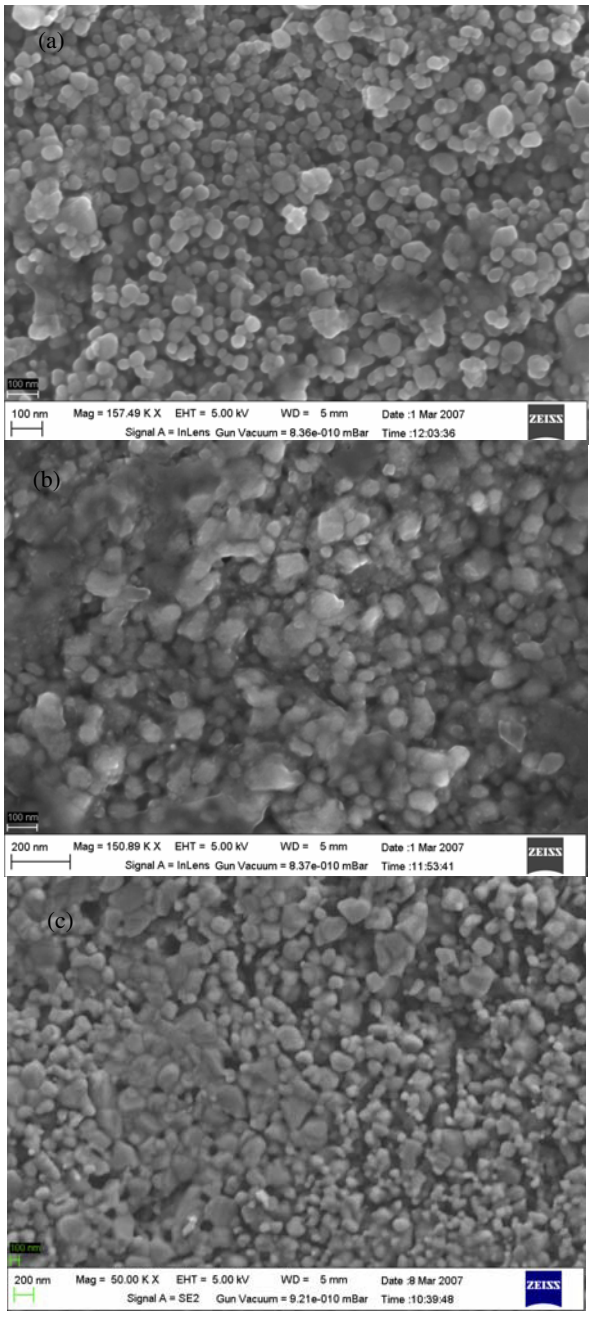

Figure 2. High resolution FE-SEM micrographs of $La_{0.7}Ba_{0.3}MnO_3$ nanoparticles calcined at (a) 850 (b) 1000 and (c) 1050 °C, respectively.

It was reported that, in an ideal monodisperse system, a single magnetic domain should be expected for manganite

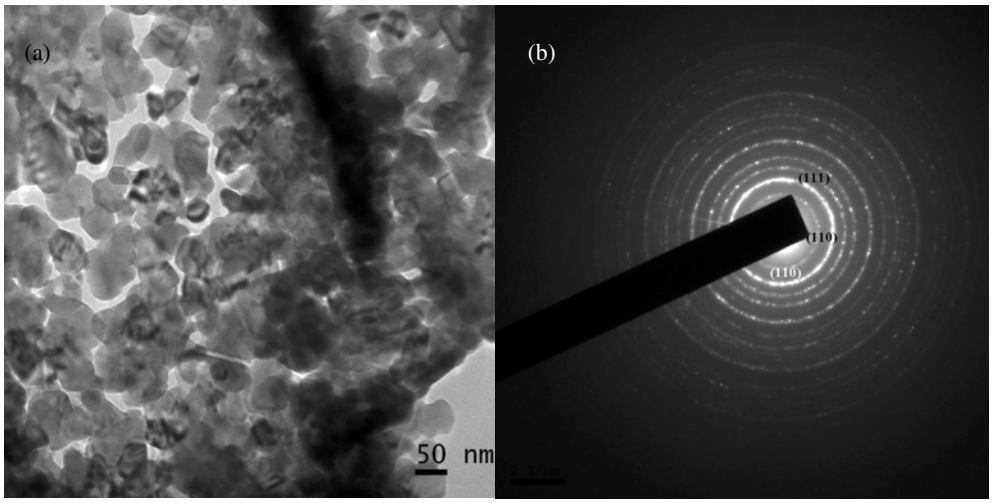

Figure 3. (a) Low magnification bright-field TEM image and (b) SAED patterns of $La_{0.7}Ba_{0.3}MnO_3$ nanoparticles calcined at 900 °C.

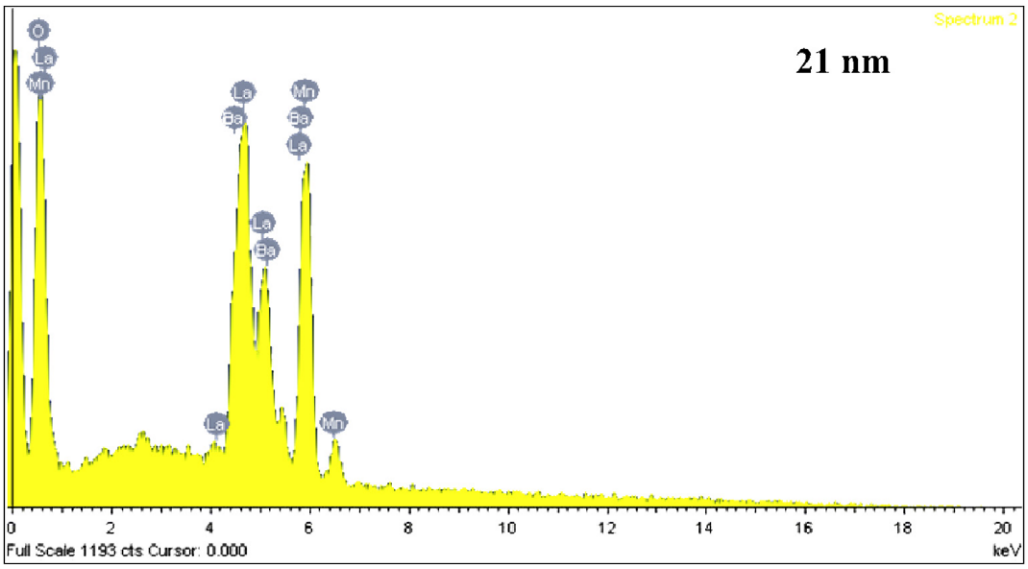

Figure 4. EDAX spectra of $La_{0.7}Ba_{0.3}MnO_3$ nanoparticles calcined at 850 °C having average grain size 21 nm.

particles with a size lower than a critical value of $D_C \sim 70$ nm [40]. Though our real system is polydisperse in nature, the reasonably narrow distribution of particle sizes, especially for the $D = 21$ nm sample (calcination temperature 850 °C), indicates that at least for our smallest grain size sample ($D = 21$ nm) the maximum particle size is not expected to cross 70 nm. That is, we can assign the nature of the physical structure of this sample ($D = 21$ nm) as an assembly of single magnetic domain particles having grain size in the nanometric regime.

3.2. Electronic-transport studies

Figure 5(a) shows the normalized resistivity (ρ) as a function of temperature for the series of LBMO nanocrystalline samples having average grain sizes 21, 25 and 30 nm. It is evident from figure 5(a) that with the decrease in average grain size the metal–insulator transition temperature (T_P) shifts towards lower temperature, associated with a pronounced increase in ρ over the entire temperature range studied. In comparison with bulk ceramic samples ($T_P = 343$ K) [22] and epitaxial thin films ($T_P \sim 245$ K) [20], for our largest grain sample ($D = 30$ nm) T_P appears at 285 K, while for our smallest grain sample ($D = 21$ nm) it appears at 240 K (as shown in table 1). A similar behavior has also been observed in the case of other nanomanganite systems [5, 37–40]. A

Table 1. Average grain size (nm), para–ferromagnetic transition temperature [T_C (K)] and metal–insulator transition temperature [T_P (K)].

Average grain size (nm)	T_C (K)	T_P (K)
21	311	240
25	313	260
30	336	285

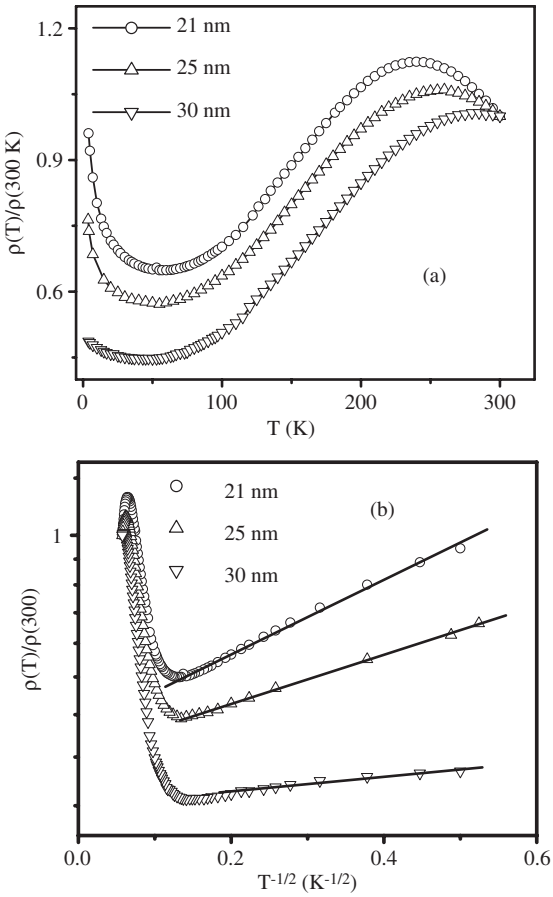

Figure 5. (a) Normalized reduced resistivity versus temperature for a series of $La_{0.7}Ba_{0.3}MnO_3$ nanoparticles having average grain sizes of 21, 25 and 30 nm in the temperature range of 4–300 K. (b) Plots of $\rho(T)/\rho(300)$ versus $1/\sqrt{T}$, where symbols are the experimental data points and the straight line denotes the low temperature resistivity fit to $\rho(T) = A\exp(\sqrt{\Delta/T})$. The slope of these fits is proportional to an electrostatic Coulomb energy barrier (E_C) between nanometric grains.

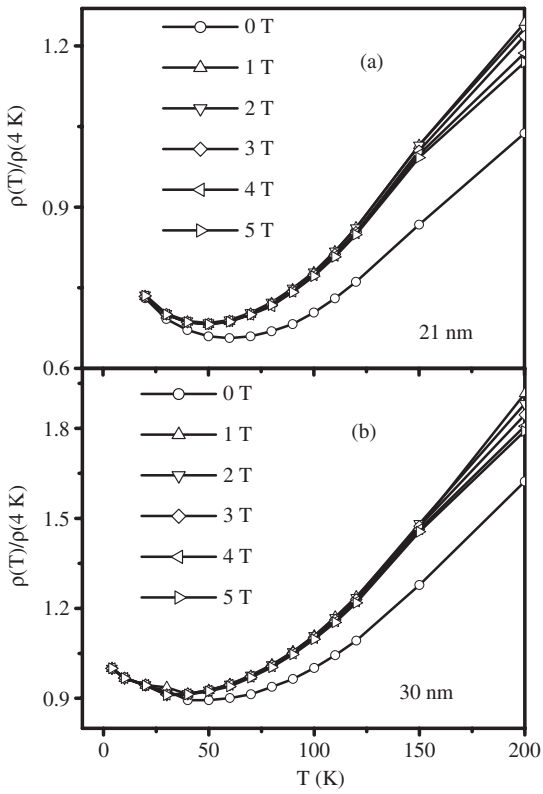

Figure 6. Plots of $\rho(T)/\rho$ (4 K) versus T of $La_{0.7}Ba_{0.3}MnO_3$ nanoparticles having average grain sizes of 21 (a) and 30 nm (b) in the temperature range of 4–200 K with applied magnetic fields of 0, 1, 2, 3, 4 and 5 T.

plausible physical explanation can be given in the light of a phenomenological model based upon an SPT mechanism, as proposed by Dey *et al* [40] for this observed electronic transport behavior of these manganite nanoparticles over the entire temperature range studied (20–300 K).

At sufficiently low temperatures (∼47 K) there is a resistivity upturn (figure 5(a)), i.e. a minimum (T_{min}) in ρ–T curves in this series of samples. Noticeably, the minima positions, i.e. T_{min} (∼47 K), are found to be almost the same for the whole series of samples. However, on decreasing the temperature by 4 K from their respective T_{min}, the rise in resistivity for the 21 nm sample is larger than for the 30 nm sample. This is another extrinsic effect that is not present in single crystals, but is common in polycrystalline ceramic samples and was also observed in the case of the nanomanganites system [40, 41]. In a previous study, Kumar *et al* [42] attributed this resistivity upturn in the case of LCMO thin films mainly to the electron–electron (e–e) interaction that considers the phase coherence of two electrons at low temperature, as a result of which both become localized through elastic impurity scattering. However, in the case of granular nanometric manganites this feature is generally explained in terms of a Coulomb blockade contribution to the resistivity [43].

In order to explain this low temperature resistivity minima and the sharper rise in resistivity for the smaller grain size sample ($D = 21$ nm) than that of the larger grain size sample ($D = 30$ nm) at low temperature, we have adopted the theoretical results as proposed by Sheng *et al* [43], according to which

$$\rho(T) \approx \exp\sqrt{(\Delta/T)} \tag{1}$$

with $\Delta \sim E_C$, where E_C is the charging energy. Figure 5(b) shows the plot of $\rho(T)/\rho(300)$ versus $T^{-1/2}$ curves for those three samples having average grain sizes 21, 25 and 30 nm up to a lowest attainable temperature down to 4 K (figure 5(b)). We have fitted the $\rho(T)/\rho(300)$ versus $T^{-1/2}$ curve at the low temperature regime of 50–4 K where resistivity exhibits an upturn as shown in figure 5(b). We obtained $E_C \sim \Delta$ from these fits as 1.3 K for the 21 nm sample, 0.56 K for the 25 nm sample and 0.04 K for the 30 nm sample. We have observed that E_C increases with the decrease in average grain size, which is in agreement with a previous study [40]. So, from these fits we may conclude that, with the decrease in average grain size the contribution of the Coulomb barrier increases [40], i.e. at a reasonably low temperature ∼47 K the net energy barrier (E) is quite large for a sufficiently small grain size sample ($D = 21$ nm). As we have already mentioned charge carriers are thermally activated, therefore,

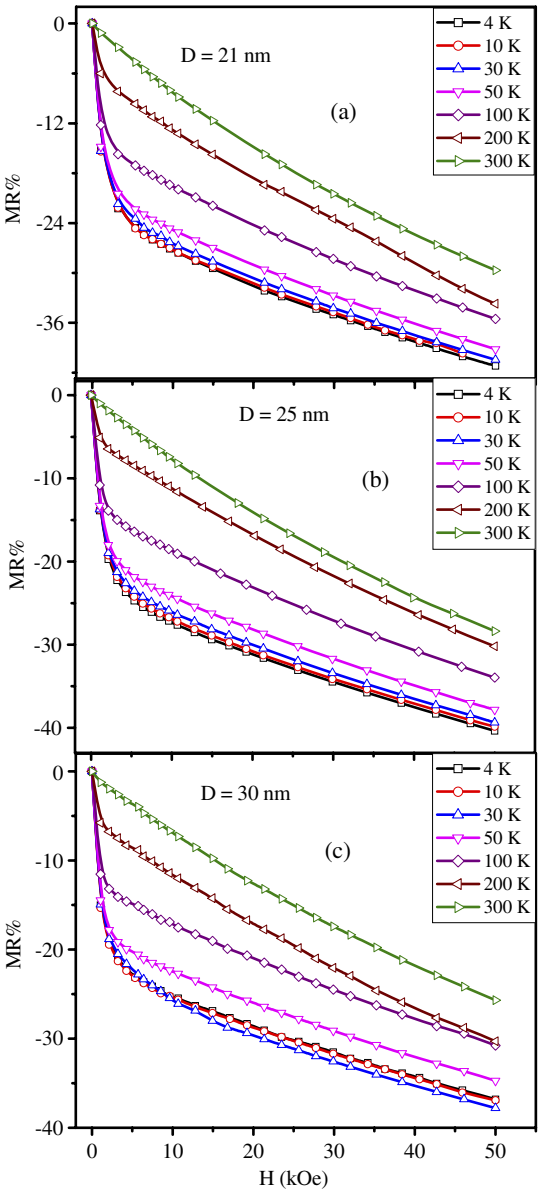

Figure 7. MR (%) plots for a series of $La_{0.7}Ba_{0.3}MnO_3$ nanoparticles having average grain sizes of 21 (a), 25 (b) and 30 nm (c) at different temperatures.

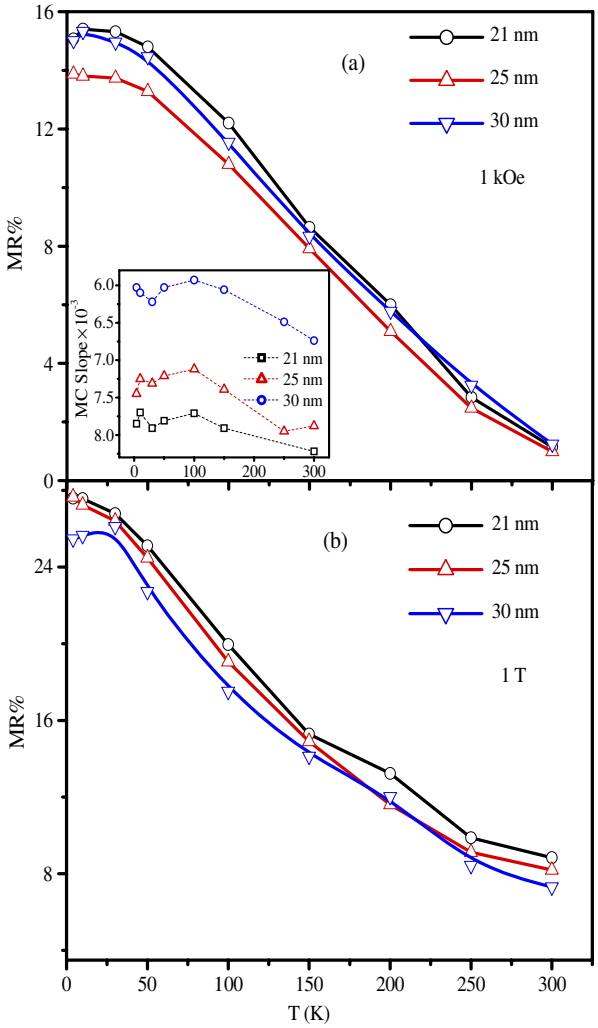

Figure 8. MR (%) versus temperature plots of $La_{0.7}Ba_{0.3}MnO_3$ nanoparticles having average grain sizes of 21, 25 and 30 nm at magnetic fields of 1 kOe (a) and 1 T (b), respectively. Inset of (a) shows the high field magnetic conductivity (MC) slope (S) as a function of temperature for LBMO samples having average grain sizes 21, 25 and 30 nm.

for nanodimensional manganites in the low temperature regime charge carriers would have considerably lower energy (E'_C) than those of E. In the very low temperature regime, though a favorable condition for SPT of conduction electrons can be achieved, charge carriers are inhibited from tunneling from grain to grain as they have insufficient energy ($E'_C \ll E$). Therefore at very low temperature there is again a pronounced increase in resistivity resulting in the observed upturn and there is a steeper rise in resistivity with the reduction of grain size.

Figures 6(a) and (b) show the $\rho(T)/\rho$ (4 K) versus temperature plots at applied magnetic fields of 0, 1, 2, 3, 4 and 5 T for average grain sizes of 21 and 30 nm, respectively. We have observed that all low temperature minima (T_{min}) at different applied magnetic fields are superimposed. It is also observed that the normalized resistivity at the applied magnetic field slightly decreases from the zero magnetic field condition. But Kumar *et al* [42] shows contrasting behavior, i.e. with an increase in applied magnetic field the depth of the resistivity minima is decreased for LCMO thin films. The upturn of normalized resistivity at lower temperature has been attributed to the electron–electron interaction effect.

3.3. Magneto-transport studies

MR measurements (figures 7(a)–(c)) show the typical magnetic field and temperature-dependent behavior of MR of LBMO nanocrystals having average grain sizes 21, 25 and 30 nm, respectively. These curves exhibit the usual behavior of polycrystalline samples with a large low field MR (LFMR, $H < 5$ kOe) at low temperatures followed by a slower varying MR at a comparatively high field (HFMR, $H > 5$ kOe), where MR is almost linear with H. We believe the observed negative MR of our nanocrystalline LBMO sample originates

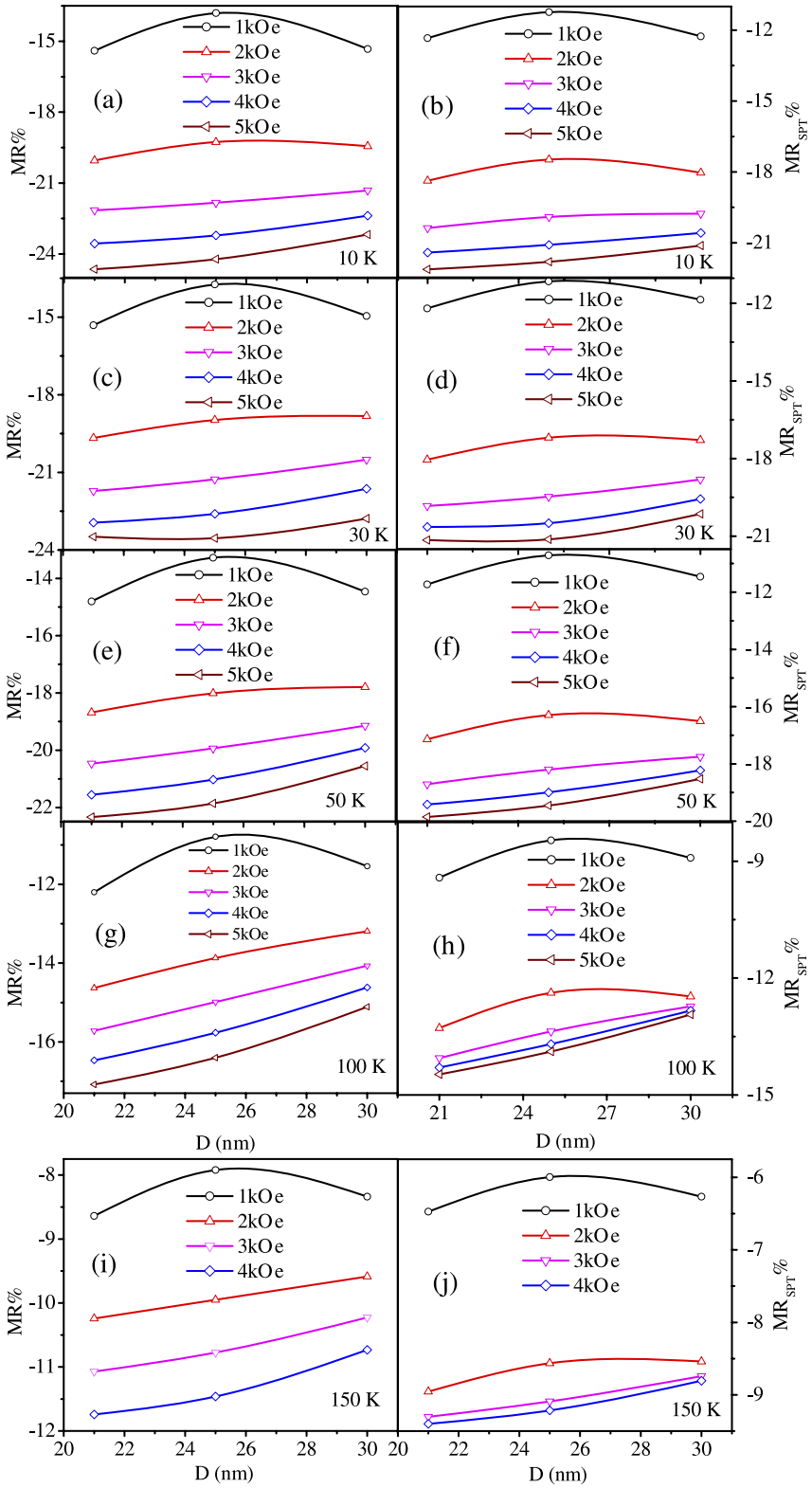

Figure 9. MR (%) versus average grain size plots ((a), (c), (e), (g) and (i)) and MR_{SPT} versus particle size plots ((b), (d), (f), (h) and (j)) of $La_{0.7}Ba_{0.3}MnO_3$ nanoparticles at different temperatures.

from two magnetic-field-dependent resistivity contributions to the system: (a) a part coming from the reduction of spin fluctuation $R_{INT}(H)$ and (b) a part coming from spin-polarized tunneling $R_{SPT}(H)$ of the conduction electrons between two adjacent grains. According to Hwang *et al* [14] LFMR in polycrystalline materials is governed by the spin-polarized transport across grain boundaries. The importance of the spin-polarized tunneling model in the case of manganites lies in

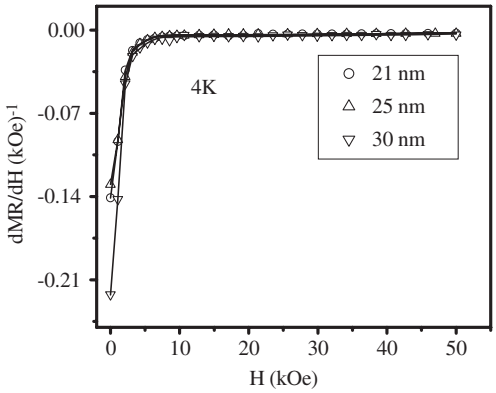

Figure 10. Field-dependent dMR/dH plots of $La_{0.7}Ba_{0.3}MnO_3$ nanoparticles having average grain sizes of 21, 25 and 30 nm at a temperature of 4 K. Fitted curves are shown as solid lines.

the fact that a relatively narrow majority carrier conduction band is completely separated from the minority band by a large Hund's energy (E_H) and an exchange energy (J_{ex}), implying a nearly complete spin polarization of the charge carriers [29] ($P \sim 100\%$). We have plotted LFMR at a magnetic field of 1 kOe and HFMR at a magnetic field of 1 T, both as a function of temperature for particle sizes 21, 25 and 30 nm as shown in figures 8(a) and (b), respectively. Both of these figures show the usual decrease in LFMR and HFMR with increase in temperature, which is in accordance with the previous literature [4, 41]. In this nanodimensional LBMO system we observed that the magnitude of LFMR as well as of HFMR remains constant almost up to a temperature of ∼50 K and then drops sharply with temperature.

In order to address this phenomenon we have adopted the theoretical perspective as was reported by Lee *et al* [15]. Hence, to analyze our data using this model, we have presented in the inset of figure 8(a) a detailed study of magneto-conductivity (MC), calculated as $MC = \sigma(H)/\sigma_0$, as a function of temperature for 21, 25 and 30 nm samples, respectively. Considering this model, the slope (S) of the MC with magnetic field curve at high field ($H >$ 20 kOe) can be taken to be the measure of the surface spin susceptibility χ_b. Very interestingly, we found that S, i.e. χ_b, follows a similar behavior to the temperature dependence of MR of the respective samples. This theoretical analysis indirectly supports our understanding of the role of the surface magnetization (M_S), which we believe to be the key factor for this unusual temperature-dependent behavior of MR in our nanodimensional manganite systems.

We have also investigated MR at magnetic fields of 1–5 kOe for varying particle sizes and at different temperatures, as shown in figures 9(a), (c), (e), (g) and (i). These figures show that, up to a magnetic field of 3 kOe, experimental MR decreases with the decrease in grain size from 30 to 25 nm. However, with a further decrease in grain size from 25 to 21 nm MR again increases. This crossover behavior of experimental MR with grain size is shared at all the temperatures, as can be clearly seen from figures 9(a), (c), (e), (g) and (i). However, beyond the 3 kOe magnetic field, on further increase in the field, the experimental MR monotonically increases

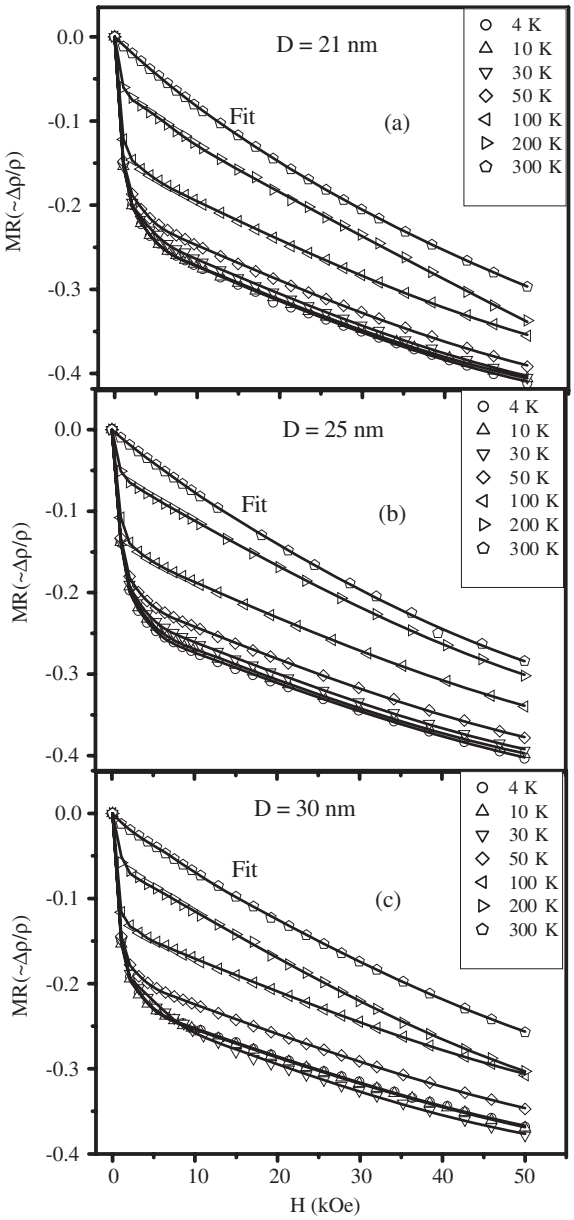

Figure 11. Field-dependent MR plots of $La_{0.7}Ba_{0.3}MnO_3$ nanoparticles having average grain sizes of 21 (a), 25 (b) and 30 nm (c) at temperatures of 4, 10, 30, 50, 100, 200 and 300 K. Fitted curves are shown as solid lines.

with increase in grain size (figures 9(a), (c), (e), (g) and (i)). In order to understand this different grain size dependence of experimental MR at different regimes of fields in our nanocrystalline LBMO sample, our approach is to separate out the part of MR originating from SPT (MR_{SPT}) from the part of the MR identified by the suppression of spin fluctuation (MR_{INT}) and mainly to inspect their respective grain size dependences. For this purpose, we have used the model as proposed by Raychaudhuri *et al* [4], based on SPT transport of conduction electrons at the grain boundaries with attention paid to the magnetic domain wall motion at grain boundaries under the application of a magnetic field. Extending the idea of SPT as proposed by Helman and Abeles [44], this model describes the magnetic field dependence of MR taking into account the

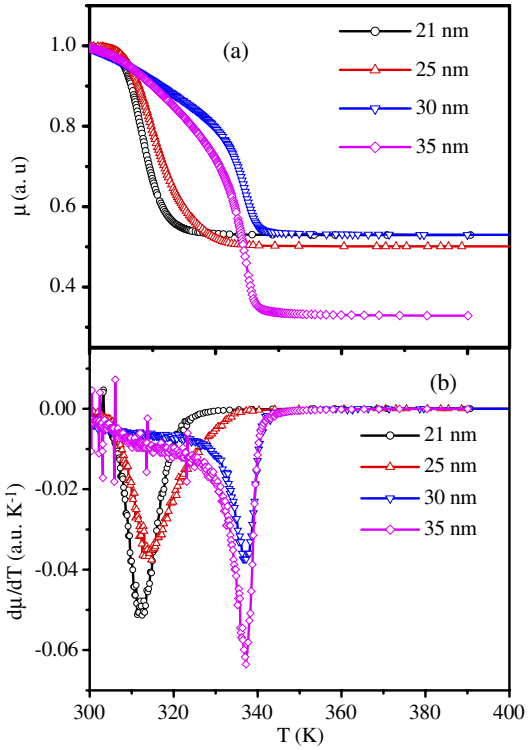

Figure 12. (a) Temperature-dependent μ curves of $La_{0.7}Ba_{0.3}MnO_3$ nanoparticles having average grain sizes of 21, 25, 30 and 35 nm, respectively. (b) Differentiation of temperature-dependent μ curves of $La_{0.7}Ba_{0.3}MnO_3$ nanoparticles having average grain sizes of 21, 25, 30 and 35 nm, respectively. From the peak position we have estimated the T_C of those samples.

gradual slippage of domain walls across the grain boundary pinning centers in an applied magnetic field. According to this model we get the expression for MR as

$$\mathrm{MR} = -A' \int_0^H f(k)\mathrm{d}k - JH - KH^3. \tag{2}$$

Within the approximation of the model, at zero field the domain boundaries are pinned at the grain boundary pinning centers having pinning strengths k. The grain boundaries have a distribution of pinning strengths (defined as the minimum field needed to overcome a particular pinning barrier) given by $f(k)$, expressed as

$$f(k) = A\exp(-Bk^2) + Ck^2\exp(-Dk^2). \tag{3}$$

All the adjustable fitting parameters, A, B, C, D, J and K, with A' absorbed in A and C, are required to be known from a nonlinear least square fitting to calculate $\mathrm{MR_{SPT}}$, which is defined as

$$\mathrm{MR_{SPT}} = -\int_0^H f(k)\mathrm{d}k. \tag{4}$$

To fit equation (2) to the MR curves for those samples having different particle sizes we have followed the same scheme as used by Raychaudhuri *et al* [4]. Differentiating equation (2) with respect to H and putting equation (3) we get

$$\frac{\mathrm{d(MR)}}{\mathrm{d}H} = A\exp(-BH^2) + CH^2\exp(-DH^2) - J - 3kH^2. \tag{5}$$

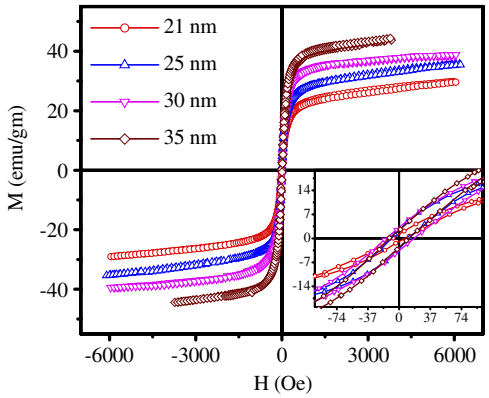

Figure 13. Field-dependent magnetization curves ($M(H)$) of $La_{0.7}Ba_{0.3}MnO_3$ nanoparticles having average grain sizes of 21, 25, 30 and 35 nm, respectively. Inset shows the expanded view of ($M(H)$) curves at $H \sim 0$ of those samples.

The experimental (MR–H) curves were differentiated and fitted to equations (5) to find the best-fit parameters at several temperatures. Figure 10 shows the differentiated curve and the best-fit function as an example of $T = 4$ K for LBMO samples having average grain sizes 21, 25 and 30 nm, respectively. Using the best-fit parameters we have fitted equation (2) to our experimental MR versus H curves at several temperatures. The excellent fit for the experimental curves to equation (2) for samples having average grain sizes 21, 25 and 30 nm at several temperatures is shown in figures 11(a)–(c), respectively.

The calculated $\mathrm{MR_{SPT}}$ (H) (using equation (4)) at $H = 1$, 2, 3, 4 and 5 kOe at different temperatures are plotted as a function of grain sizes as shown in figures 9(b), (d), (f), (h) and (j). We have observed that $\mathrm{MR_{SPT}}$ also shows a similar dependence on grain sizes in different regimes of field as that of experimental MR (figure 9). This similar qualitative behavior of experimental MR and $\mathrm{MR_{SPT}}$ clearly indicates that it is the modulation of the SPT mechanism with varying grain sizes that gives rise to this behavior. However, in the present framework it is not possible to shed further light on this issue. A spin-polarized photoemission study is needed for a better understanding of this grain size dependence of MR.

3.4. Magnetic study

Temperature-dependent μ plots for average grain sizes of 21, 25, 30 and 35 nm are shown in figure 12(a). Differential plots of figure 12(a) are shown in figure 12(b), from which we have estimated the Curie temperature (T_C) (as shown in table 1) for those samples. The permeability μ is proportional to the magnetic susceptibility (χ). We have observed that values of T_C shift to lower temperature with decreasing average grain size. Similar behavior is also observed for LCMO nanoparticles [5, 37] and [41]. Field-dependent magnetization ($M(H)$) curves at room temperature for average grain sizes of 21, 25, 30 and 35 nm are shown in figure 13. The magnified portion of those curves in the low field region as $H \sim 0$ is shown in the inset of figure 13. The rising portion of the $M(H)$ curves, i.e. the field range of 0–+4 kOe for average grain

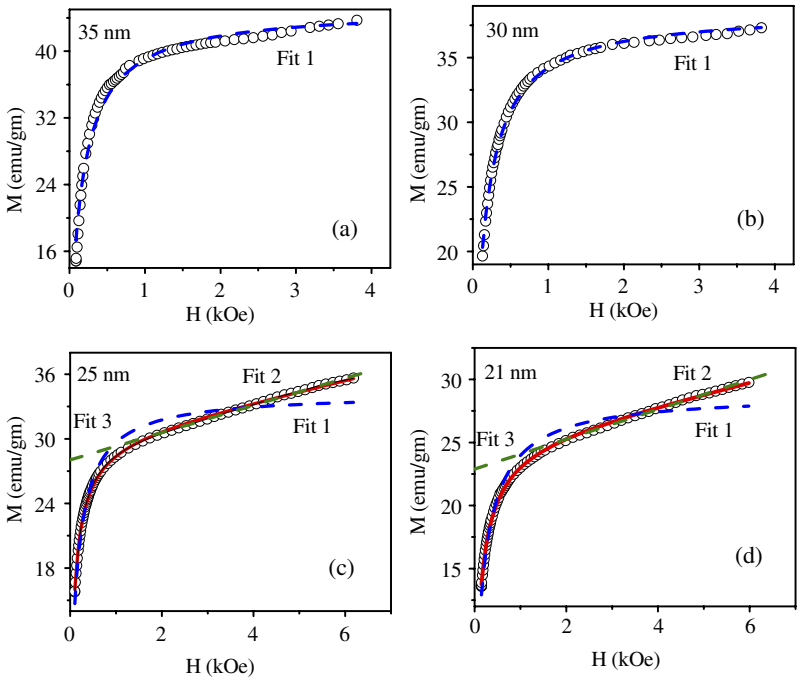

Figure 14. (a) and (b) $M(H)$ plots of $La_{0.7}Ba_{0.3}MnO_3$ nanoparticles having average grain sizes of 35 and 30 nm, respectively. These curves are fitted with the Brillouin function [Fit 1] as shown by dotted curves. (c) and (d) $M(H)$ plots of $La_{0.7}Ba_{0.3}MnO_3$ nanoparticles having average grain sizes of 25 and 21 nm, respectively. These curves are fitted with the Brillouin function [Fit 1] (blue), Brillouin and paramagnetic function [Fit 2] (red) and paramagnetic function [Fit 3] (green).

sizes of 35 (as shown in figure 14(a)) and 30 nm (as shown in figure 14(b)), fits well [Fit 1] ($\chi^2 = 0.014\,64$, $R^2 = 0.985\,36$ for the grain size 35 nm and $\chi^2 = 0.0795$, $R^2 = 0.996\,97$ for the grain size 30 nm) with the Brillouin function as

$$M = M_{\text{Ferro}} = a\tanh(\mu H/kT) \tag{6}$$

where a is the fit parameter and μ is the mean moment. However, in the lower grain size cases (25 nm for figure 14(c) and 21 nm for figure 14(d)), we have fitted those curves once considering only the Brillouin function term [Fit 1] and then the Brillouin function with an extra paramagnetic term [Fit 2] as defined as

$$\begin{aligned} M &= M_{\text{Ferro}} + M_{\text{Para}} \\ M &= a\tanh(\mu H/kT) + bH \end{aligned} \tag{7}$$

where b is the fit parameter and bH is the paramagnetic term. Similar kinds of both paramagnetic and superparamagnetic fitting terms have also been considered by Toro *et al* [45] on $M(H)$ curves of a nanocrystalline $Fe_{61}Re_{30}Cr_9$ alloy. We have also attempted to fit the $M(H)$ curve of figures 14(c) and (d) using a paramagnetic component only [Fit 3] ($R^2 = 0.9969$ for grain size 25 nm and $R^2 = 0.9956$ for grain size 21 nm) as shown in figures 14(c) and (d), respectively. The fitting of the paramagnetic term does not improve the quality of the fit. From those fits, we have clearly observed that Fit 2 fits better ($\chi^2 = 0.012\,47$, $R^2 = 0.9996$ for grain size 25 nm and $\chi^2 = 0.008\,45$, $R^2 = 0.999\,66$ for grain size 21 nm) than other fits (for Fit 1, $\chi^2 = 0.983\,86$, $R^2 = 0.967\,77$ for grain size 25 nm and $\chi^2 = 0.651\,76$, $R^2 = 0.973\,67$ for grain size 21 nm). This can be attributed to that, in lower grain size samples, the grain boundary thickness is larger than for higher grain size. Thus a large number of surface spins should reside at the grain boundary which behaves as the paramagnetic component of those systems.

Figures 15(a) and (b) show the temperature-dependent magnetization [$M(T)$] curves at zero-field-cooled (ZFC) and field-cooled warming (FCW) conditions at an applied dc magnetic field (H_{dc}) of 500 Oe for average grain sizes of 21 and 30 nm, respectively. The expanded view in the low temperature region at the FCW condition for the 21 nm sample is shown in the inset of figure 15(a). The peak position (T_{max}) of this curve is found to be 84 K. On the other hand, the almost plateau-like shape of the FCW curve (in superparamagnets the FCW branch keeps increasing monotonically [45]) is observed in the FCW condition for the average grain size 30 nm sample as shown in the inset of figure 15(b). However, this feature has been recently found not to be exclusive to spin glasses, but also shared by fine particle systems with random anisotropy and strong dipole–dipole interaction [45–48]. Such a result is also reported from a Monte Carlo simulation where it is shown that the particles size distribution does not affect such behavior [49].

4. Conclusions

In conclusion we have synthesized LBMO nanoparticles through a chemical 'pyrophoric reaction process' having average grain sizes of 21–35 nm. From high resolution FE-SEM and TEM micrographs, the particle sizes were found

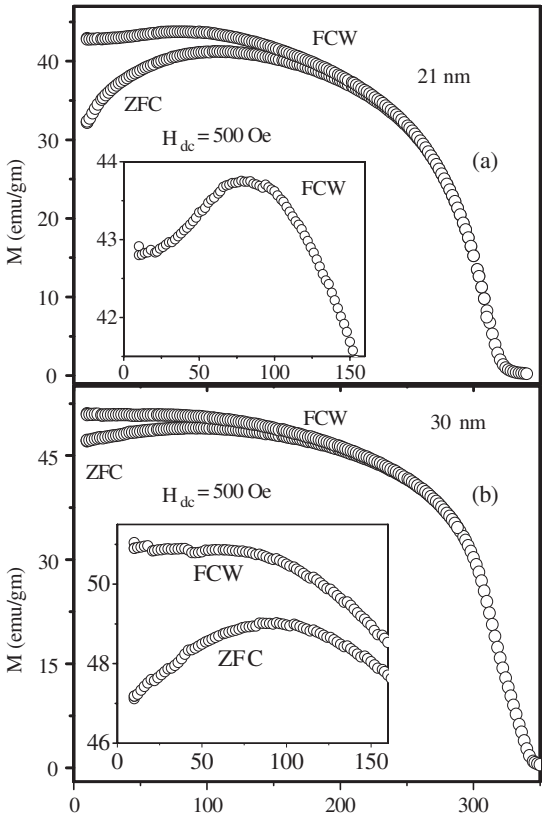

Figure 15. (a) Temperature-dependent magnetization ($M(T)$) plot of $La_{0.7}Ba_{0.3}MnO_3$ nanoparticles having an average grain size of 21 nm in zero-field-cooled (ZFC) and field-cooled warming (FCW) at a applied dc magnetic field of 500 Oe. Inset shows the expanded view of the FCW curve in the low temperature region. (b) $M(T)$ plot of $La_{0.7}Ba_{0.3}MnO_3$ nanoparticles having an average grain size of 30 nm in ZFC and FCW at a applied dc magnetic field of 500 Oe. Inset shows the expanded view of ZFC and FCW curves in the low temperature region.

to be in the nanometric regime. From electronic transport studies, we have observed that T_P shifts towards lower temperature with a decrease in average grain size along with a pronounced increase in resistivity. The charging energy decreases with increase in average grain size. The observed MR of a series of LBMO nanoparticles has been explained in light of a spin-polarized tunneling mechanism. The variation of experimental LFMR with grain size at different temperatures agrees with the variation of estimated values of the spin-polarized tunneling MR contribution with grain sizes. Magneto-transport measurements show that the magnitude of LFMR, as well as of HFMR, remains constant up to sufficiently high temperature (∼50 K) and then drops sharply with temperature. This strange temperature dependence of MR is observed to be decided predominantly by the nature of the temperature response of M_S. The strong freezing of Mn spins into a distorted state, due to random exchange interactions or random anisotropies at the surface, causes such a remarkable temperature-dependent behavior of MR in these granular nanometric manganites. We have observed that T_C of those nanoparticles shifts to lower temperature with a decrease in average grain size. The $M(T)$ behavior of these samples signifies fine particle systems with random anisotropy and strong dipole–dipole interactions.

Acknowledgments

The authors acknowledge the DST-NSTI project (no. SR/S5/NM-04/2005), India, for financial support. One of us (TKN) would like to acknowledge the financial support from BRNS-DAE, India through project no. 2006/37/52/BRNS/822.

References

[1] Jonker G H and Van Santen J H 1950 *Physica* **16** 337
[2] Wollan E O and Koehler W C 1951 *Phys. Rev.* **100** 545
Zener C 1951 *Phys. Rev.* **82** 403
[3] Hwang H Y, Cheong S-W, Ong N P and Batlogg B 1996 *Phys. Rev. Lett.* **77** 2041
[4] Raychaudhuri P, Sheshadri K, Taneja P, Bandyopadhyay S, Ayyub P, Nigam A K and Pinto R 1999 *Phys. Rev.* B **59** 13919
Raychaudhuri P, Nath T K, Nigam A K and Pinto R 1998 *J. Appl. Phys.* **84** 2048
[5] Rivas J, Hueso L E, Fondado A, Rivadulla F and López-Quintela M A 2000 *J. Magn. Magn. Mater.* **221** 57
[6] Lamas D G, Caneiro A, Niebieskikwiat D, Sánchez R D, García D and Alascio B 2002 *J. Magn. Magn. Mater.* **241** 207
[7] Zhang N, Ding W, Zhong W, Xing D and Du Y 1997 *Phys. Rev.* B **56** 8138
[8] Okuda T, Asamitsu A, Tomioka Y, Kimura T, Taguchi Y and Tokura Y 1998 *Phys. Rev. Lett.* **81** 3203
[9] Zhou J-S, Goodenough J B, Asamitsu A and Tokura Y 1997 *Phys. Rev. Lett.* **79** 3234
[10] Rao R A, Lavric D, Nath T K, Eom C B, Wu L and Tsui F 1998 *Appl. Phys. Lett.* **73** 3294
[11] Suzuki Y, Hwang H Y, Cheong S W and vanDover R B 1997 *Appl. Phys. Lett.* **71** 140
[12] Kwon C W, Robson M C, Kim K-C, Gu J Y, Lofland S E, Bhagat S M, Trajanovic Z, Rajeswari M, Venkatesan T, Kratz A R, Gomez R D and Ramesh R 1997 *J. Magn. Magn. Mater.* **172** 229
[13] Mahendiran R, Tiwary S K, Raychaudhuri A K, Ramakrishnan T V, Mahesh R, Rangavittal N and Rao C N R 1996 *Phys. Rev.* B **53** 3348
[14] Hwang H Y, Cheong S-W, Radaelli P G, Marezio M and Batlogg B 1995 *Phys. Rev. Lett.* **75** 914
[15] Lee S, Hwang H Y, Shraiman B I, Ratcliff II W D and Cheong S-W 1999 *Phys. Rev. Lett.* **82** 4508
[16] Urushibara A, Moritomo Y, Arima T, Asamitsu A, Kido G and Tokura Y 1995 *Phys. Rev.* B **51** 14103
[17] Ju H L, Gopalkrishnan J, Peng J L, Li Qi, Xiong G C, Venkatesan T and Greene R L 1995 *Phys. Rev.* B **51** 6143
[18] Rodriguez-Martinez Lide M and Paul Attfield J 1996 *Phys. Rev.* B **54** R15622
[19] Uehara M, Mori S, Chen C H and Cheong S W 1999 *Nature* **399** 560
[20] von Helmolt R, Wecker J, Holzapfel B, Schultz L and Samwer K 1993 *Phys. Rev. Lett.* **71** 2331 and references therein
[21] Shannon R D 1976 *Acta Crystallogr.* A **32** 751
[22] Ju H L, Nam Y S, Lee J E and Shin H S 2000 *J. Magn. Magn. Mater.* **219** 1
[23] Trukhanov S V, Lobanovski L S, Bushinsky M V, Troyanchuk I O and Szymczak H 2003 *J. Phys.: Condens. Matter* **15** 1783
[24] Demin R V, Koroleva L I and Mukovskii Y M 2005 *J. Phys.: Condens. Matter* **17** 221
[25] Zhu D, Zhu H and Zhang Y 2002 *Appl. Phys. Lett.* **80** 1634

[26] Dey P, Nath T K, Kumar U and Mukhopadhyay P K 2005 *J. Appl. Phys.* **98** 014306
[27] Lamas D G, Caneiro A, Niebieskikwiat D, Sánchez R D, García D and Alascio B 2002 *J. Magn. Magn. Mater.* **241** 207–13
[28] Zhang N, Ding W, Zhong W, Xing D and Du Y 1997 *Phys. Rev.* B **56** 8138
[29] Savosta M M, Krivoruchko V N, Danilenko I A, Tarenkov V Yu, Konstantinova T E, Borodin A V and Varyukhin V N 2004 *Phys. Rev.* B **69** 024413
[30] Balcells L1, Martínez B, Sandiumenge F and Fontcuberta J 2000 *J. Magn. Magn. Mater.* **211** 193
[31] Zhu T, Shen B G, Sun J R, Zhao H W and Zhan W S 2001 *Appl. Phys. Lett.* **78** 3863
[32] Duan Y W, Kou X L and Li J G 2005 *Physica* B **355** 250
[33] Ji T, Fang J, Golob V, Tang J and O'Connor C J 2002 *J. Appl. Phys.* **92** 6833
[34] Niebieskikwiat D, Sánchez R D, Lamas D G, Caneiro A, Hueso L E and Rivas J 2003 *J. Appl. Phys.* **93** 6305
[35] Dutta A, Gayathri N and Ranganathan R 2003 *Phys. Rev.* B **68** 054432
[36] Mahesh R, Mahendiran R, Raychaudhuri A K and Rao C N R 1996 *Appl. Phys. Lett.* **68** 2291
[37] Sánchez R D, Rivas J, Vázquez-Vázquez C, López-Quintela A, Causa M T, Tovar M and Oseroff S 1996 *Appl. Phys. Lett.* **68** 134
[38] Hueso L E, Rivadulla F, Sánchez R D, Caeiro D, Jardón C, Vázquez-Vázquez C, Rivas J and López-Quintela M A 1998 *J. Magn. Magn. Mater.* **189** 321–8
[39] Sánchez R D, Rivas J, Caeiro D, Östlund M, Servin M, Vázquez C, López-Quintela M A, Causa M T and Oseroff S B 1997 *Mater. Sci. Forum* **831** 235–8
[40] Dey P and Nath T K 2006 *Phys. Rev.* B **73** 214425
[41] López-Quintela M A, Hueso L E, Rivas J and Rivadulla F 2003 *Nanotechnology* **14** 212
[42] Kumar D, Sankar J, Narayan J, Singh R K and Majumdar A K 2002 *Phys. Rev.* B **65** 094407
[43] Sheng P, Abeles B and Arie Y 1973 *Phys. Rev. Lett.* **31** 44
[44] Helman J S and Abeles B 1976 *Phys. Rev. Lett.* **37** 1429
[45] De Torro J A, Lopez de la Torre M A, Arranz M A, Riveiro J M, Martinez J L, Palade P and Filoti G 2001 *Phys. Rev.* B **64** 094438
[46] Bitoh T, Ohba K, Takamatsu M, Shirane T and Chikazawa S 1995 *J. Phys. Soc. Japan* **64** 1305
[47] Mamiya H, Nakatani I and Furubayashi T 1998 *Phys. Rev. Lett.* **80** 177
[48] Batlle X, García del Muro M and Labarta A 1997 *Phys. Rev.* B **55** 6440
[49] García-Otero J, Porto M, Rivas J and Bundez A 2000 *Phys. Rev. Lett.* **84** 167